

Article

Reliability-Based Topology Optimization of Thermo-Elastic Structures with Stress Constraint

Liang Zhang ¹, Qinghai Zhao ^{1,2,*} and Jianliang Chen ¹

¹ School of Mechanical and Electrical Engineering, Qingdao University, Qingdao 266071, China; 2020025584@qdu.edu.cn (L.Z.); 2020020438@qdu.edu.cn (J.C.)

² National Engineering Research Center for Intelligent Electrical Vehicle Power System, Qingdao University, Qingdao 266071, China

* Correspondence: zhaoqh@qdu.edu.cn

Abstract: Traditional topology optimization of thermo-elastic structures is based on deterministic conditions, without considering the influence of uncertainty factors. To address the impact uncertainty on structural strength, a reliability-based topology optimization of thermo-elastic structure with stress constraint is proposed. The probabilistic uncertainty quantities are associated with the structural material property, mechanical loads and the thermal stress coefficient with the topology optimization formulation considering volume minimization and stress constraint. The relaxation stress method combined with normalized p-norm function is adopted to condense whole element stresses into the global stress measurement that approximates the maximum stress. The adjoint variable method is utilized to derive the sensitivity of the stress constraint and the optimization problem is solved by the method of moving asymptote (MMA). Finally, several numerical examples are presented to demonstrate the effectiveness and validity of the proposed approach. Compared with the deterministic design, the reliability design has distinct topological configurations and the optimized structures maintain a higher reliability level.



Citation: Zhang, L.; Zhao, Q.; Chen, J. Reliability-Based Topology Optimization of Thermo-Elastic Structures with Stress Constraint. *Mathematics* **2022**, *10*, 1091. <https://doi.org/10.3390/math10071091>

Academic Editors: Fajie Wang, Ji Lin and Armin Fügenschuh

Received: 4 March 2022

Accepted: 24 March 2022

Published: 28 March 2022

Publisher's Note: MDPI stays neutral with regard to jurisdictional claims in published maps and institutional affiliations.



Copyright: © 2022 by the authors. Licensee MDPI, Basel, Switzerland. This article is an open access article distributed under the terms and conditions of the Creative Commons Attribution (CC BY) license (<https://creativecommons.org/licenses/by/4.0/>).

Keywords: thermo-elastic structure; topology optimization; reliability analysis; stress constraint

MSC: 65K10

1. Introduction

Various mechanical parts, such as turbines, rockets and battery systems, are subjected to both thermal and mechanical loads because of the working environment with coupled temperature and structural fields. In this scenario, it is necessary for the thermo-elastic design to consider the temperature factor's impact on structural strength to prevent structural failure [1].

In recent years, topology optimization methods are widely used in thermo-elastic structure design, including the variable density method, the homogenization method, the evolutionary optimization method, the level set method, etc. Rodrigue et al. [2] first proposed the topology optimization of thermo-elastic structures by the homogenization method. Du et al. [3] performed the topology optimization of thermal-driven compliant mechanisms by the variable density method. Li et al. [4] conducted a study on the optimal design of thermo-elastic structures under the non-uniform temperature field based on the evolutionary optimization method. Deng et al. [5] used the level set method to derive the topological sensitivity information for the thermo-elastic structures. Most of the studies in the above-mentioned literature are based on the compliance minimization, while the strength is an essential design criterion in engineering practice. Recently, it has been stated in Ref. [6] that the topology optimization model of compliance minimization is not suitable for thermo-elastic topology optimization, because when the temperature load is comparable to the mechanical load, compliance minimization cannot obtain an optimal structure with

reasonable strength. More researches have illustrated that simple reinforcement techniques cannot sufficiently solve the problem of thermo-elastic structural strength failure caused by destructive stress [7]. Therefore, stress-based topology optimization design is necessary and has been gradually emerged.

Topology optimization related with stress constraint is the most challenging research field. This is mainly due to the following three problems: (i) the singularity problem, (ii) the local nature of stresses, and (iii) the highly nonlinear behavior of stress constraints [8]. According to the relevant literature, there are some efficient approaches to deal with the above-mentioned problems. Regarding the singular phenomenon, the commonly used methods include ε -relaxation techniques [9,10], qp-relaxation techniques [11,12], etc. For the local nature of stress, local stress constraints are transformed into global stress constraint by using aggregation function, including the p-norm [13,14] and KS-function [15]. In addition to the above numerical problems, the third challenge is the highly nonlinear stress behavior wherein stress distribution is highly sensitive to even subtle topological variations, particularly at critical regions with high stress concentration [16]. This feature is reflected in the tendency of the optimization iterations to have repeated oscillations. To stabilize the convergence, a density filtering method and suitable optimization solution algorithm were adopted by Le et al. [17]. Recently, Deaton et al. [18] investigated the topology optimization problem of thermo-elastic structures under stress constraint. However, the above studies on topology optimization considering stress constraint are based on deterministic topology optimization (DTO). In practical engineering, the material properties and the mechanical loads are often uncertain due to the differences of the internal conditions and the time-varying nature of the external environment. These uncertainties may affect the reliability of the structural performance and even lead to failure [19–21]. Thus, reliability-based topology optimization (RBTO) is becoming more and more prominent.

According to the different mathematical tools used to describe the properties of uncertainty, uncertainty can be divided into stochastic uncertainty and epistemic uncertainty. The former describes the inherent variability in the physical system or working environment, also known as objective uncertainty, and usually uses probabilistic methods to model random variables or stochastic processes, while the latter is mainly due to subjective knowledge limitations or incomplete information. The resulting, also known as subjective uncertainty, can be modeled by non-probabilistic methods such as fuzzy analysis [22]. Therefore, reliability topology optimization considering uncertainty conditions is mainly divided into probabilistic and non-probabilistic types. At present, the research on reliability topology optimization design with random variables as a probability distribution is relatively mature. Kharmanda et al. [23] first combined structural reliability analysis with deterministic topology optimization and established an effective reliability flowchart for structural strain energy minimization. Jung et al. [24] investigated the reliability topology optimization for the three-dimensional geometric nonlinear structure design. Zhao et al. [25] studied the multi-material topology optimization problem with reliability constraints considering the effects of incomplete measurement of structures, inaccurate information, and insufficient cognition on structures. For practical engineering applications, Silva et al. [26] adopted a single-loop topology optimization mathematical model of components and systems and applied it to the design of automotive control arms, and the results showed that the method has good practicality and efficiency.

To the author's knowledge, this is the first attempt to reliability-based topology optimization of thermo-elastic structure with stress constraint. The material property, thermal stress coefficient and mechanical loads are chosen as uncertainty variables with the probability distributions. Based on probability theory, the structural topology optimization design method considering stress constraint is combined with the existing reliability structural topology optimization model [27]. A reliability-based topology optimization design method for thermo-elastic structures under global stress constraint is proposed. The RBTO and the DTO design are compared to verify the effectiveness and feasibility of the proposed method.

2. Finite Element Formulation of Thermo-Elastic Structure

Figure 1 illustrates the generalized design domain Ω for the thermo-elastic structure problem, which consists of the predefined design domain containing the fixed displacement boundary Γ_d , surface mechanical load F^m applied on the boundary Γ_f , and the uniform temperature variation $\Delta T(x, y)$. In addition, the isotropic material is considered and the design domain is discretized into quadrilateral elements and eight-node hexahedral elements in 2D and 3D problems, respectively.

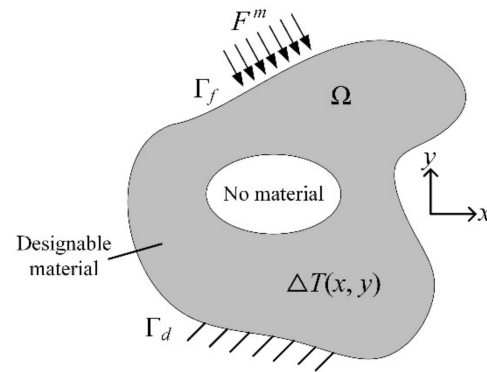


Figure 1. Generalized design domain of thermo-elastic structure.

For the thermo-elastic structure coupled with temperature and mechanical loads, the static equilibrium equations can usually be expressed as

$$K(\rho)U(\rho) = F^m + F^{th}(\rho) \tag{1}$$

where ρ is the density variable vector, $K(\rho)$ is the structural global stiffness matrix, $U(\rho)$ is the structural nodal displacement vector, F^m is the mechanical load vector, and $F^{th}(\rho)$ is the temperature load vector due to thermal strain. The stiffness matrix $K(\rho)$ is assembled by

$$K(\rho) = \sum_{e=1}^{N_e} \int_{\Omega_e} B_e^T D_e(\rho_e) B_e h d\Omega_e \tag{2}$$

where N_e is the total element number, Ω_e represents the element domain, h is the thickness of the planar element, B_e is the element strain-displacement matrix, $D_e(\rho_e)$ is the material elasticity matrix of element e [28]. Adopting the SIMP material interpolation method, $D_e(\rho_e)$ can be expressed as a function of the material elastic modulus, defined by

$$D_e(\rho_e) = E(\rho_e)D_0 = \rho_e^\alpha E_0 D_0 \tag{3}$$

where $E(\rho_e)$ is the elastic modulus of element e , α is the elastic modulus penalty factor, E_0 is the elastic modulus of the solid material, D_0 is the coefficient matrix for an element with unit elastic modulus.

The temperature load $F^{th}(\rho)$ can be assembled by accumulating the element temperature load, defined as

$$F^{th}(\rho) = \sum_{e=1}^{N_e} E(\rho_e) \int_{\Omega_e} B_e^T D_0 \epsilon_e^{th}(\rho_e) d\Omega_e \tag{4}$$

where

$$\epsilon_e^{th}(\rho_e) = \gamma(\rho_e) \Delta T \phi \tag{5}$$

where $\epsilon_e^{th}(\rho_e)$ is the thermal strain vector for the element, $\gamma(\rho_e)$ is the material thermal expansion coefficient, ΔT is the amount of uniform variation of the temperature, ϕ is defined as $[1, 1, 0]^T$ in 2D problems and $[1, 1, 1, 0, 0, 0]^T$ in 3D problems. Substituting Equation (6) into Equation (5) yields

It is noted that $E(\rho_e)$ and $\gamma(\rho_e)$ are both concerned with the element density variables. Hence, by using the thermal stress coefficient (TSC) [29], the parameters are combined into the single thermal stress coefficient, defined as

$$\delta(\rho_e) = E(\rho_e)\gamma_0\rho_e = \rho_e^k E_0\gamma_0 = \rho_e^k \delta_0 \tag{6}$$

where γ_0 is the expansion coefficient of the solid material, k is the thermal stress penalty factor, δ_0 is the thermal stress coefficient of the solid material.

Substituting Equations (5) and (6) into Equation (4), $F^{th}(\rho)$ can be expressed as

$$F^{th}(\rho) = \sum_{e=1}^{N_e} \delta(\rho_e)\Delta T \int_{\Omega_e} B_e^T D_0 \phi d\Omega_e \tag{7}$$

3. Deterministic Topology Optimization of Thermo-Elastic Structure

3.1. Mathematical Model of Deterministic Topology Optimization

With regard to the deterministic topology optimization of the thermo-elastic structure problem, the volume minimization and stress constraint are considered to satisfy the static strength failure and lightweight design. The deterministic topology optimization of the thermo-elastic structure can be established as

$$\left\{ \begin{array}{l} \text{find } \rho \\ \min V(\rho) = \sum_{e=1}^{N_e} \rho_e v_e \\ \text{s.t. } \mathbf{K}(\rho)\mathbf{U}(\rho) = \mathbf{F}^m + \mathbf{F}^{th}(\rho) \\ \sigma_e^{VM}(\rho) \leq \sigma_s \quad (e = 1, 2, \dots, N_e) \\ 0 < \rho_{min} \leq \rho_e \leq 1 (e = 1, 2, \dots, N_e) \end{array} \right. \tag{8}$$

where ρ is the density variable vector, $V(\rho)$ is the overall structural volume, v_e is the element volume, $\sigma_e^{VM}(\rho)$ is the von Mises stress of each element, σ_s is the material yield strength, and ρ_{min} is the lower limit of the design variable.

3.2. Global Stress Constraint

The topological optimization of the stress-constrained structure appears as a singular solution phenomenon, i.e., the density of the element tends to zero, yet the stress of the element is a non-zero value. To solve the singular solution phenomenon, based on the SIMP material interpolation model, the stress relaxation method is used to penalize the element stresses in the form of

$$\sigma_e(\rho) = \rho_e^q \sigma_{e0} \tag{9}$$

where $\sigma_e(\rho)$ is the interpolated element stress, q is the intensity penalty factor, and σ_{e0} is the stress vector at the center of the e th element, defined as

$$\sigma_{e0} = E_0(D_0 B_e U_e - D_0 \gamma_0 \phi \Delta T) \tag{10}$$

where U_e is the nodal displacement vector of the element. The element stress vector σ_{e0} in 2D and 3D problems is respectively expressed as

For 2D problems,

$$\sigma_{e0} = [\sigma_{ex}, \sigma_{ey}, \tau_{exy}] \tag{11}$$

For 3D problems,

$$\sigma_{e0} = [\sigma_{ex}, \sigma_{ey}, \sigma_{ez}, \tau_{exy}, \tau_{eyz}, \tau_{ezx}] \tag{12}$$

where σ_{ex} , σ_{ey} and σ_{ez} are the stress components in the x , y and z directions of element e , respectively. τ_{exy} , τ_{eyz} , and τ_{ezx} are the shear stress components on the xy , yz , and zx planes of the element e , respectively.

The fourth strength theorem is used as the failure criterion of the material, the von Mises stress σ_e^{VM} of the element can be obtained from the three components of the element stress vector, expressed as

$$\sigma_e^{VM} = \sqrt{\sigma_e^T M \sigma_e} \tag{13}$$

The Stress coefficient matrix M , in 2D and 3D problems are respectively expressed as

For 2D problems,

$$\text{For 2D problems, } M = \begin{bmatrix} 1 & -1/2 & 0 \\ -1/2 & 1 & 0 \\ 0 & 0 & 3 \end{bmatrix} \tag{14}$$

For 3D problems,

$$M = \begin{bmatrix} 1 & -1/2 & -1/2 & 0 & 0 & 0 \\ -1/2 & 1 & -1/2 & 0 & 0 & 0 \\ -1/2 & -1/2 & 1 & 0 & 0 & 0 \\ 0 & 0 & 0 & 3 & 0 & 0 \\ 0 & 0 & 0 & 0 & 3 & 0 \\ 0 & 0 & 0 & 0 & 0 & 3 \end{bmatrix} \tag{15}$$

In order to reduce the problem of computational burden caused by numerous local stress constraints, the p-norm function is adopted to construct the global stress constraint, denoted as

$$\sigma^{PN} = \left(\sum_{e=1}^{N_e} \left(\frac{\sigma_e^{VM}}{\sigma_s} \right)^p \right)^{\frac{1}{p}} \tag{16}$$

where p is the aggregation parameter. Note that p tends to infinity, and σ^{PN} is equivalent to $\max(\sigma_e^{VM}/\sigma_s)$. The stress constraint is equivalent to the global stress constraint, defined as

$$\sigma^{PN} \leq 1 \tag{17}$$

However, when p enlarges, the degree of nonlinearity of the aggregation function increases that leads to oscillation convergence in the optimization process. Otherwise, with smaller p , the aggregation function cannot capture the maximum of the stress [30]. To overcome this defect, a revised coefficient is introduced into the constraint equation, expressed as

$$\bar{\sigma}^{PN} = c\sigma^{PN} \leq 1 \tag{18}$$

where c is the revised coefficient, and before each optimization process, is defined as

$$c = \frac{\max(\sigma_e^{VM})}{\sigma_s \cdot \sigma^{PN}} \tag{19}$$

4. Reliability-Based Topology Optimization of Thermo-Elastic Structure

4.1. Reliability-Based Topology Optimization Problem Description

Reliability is an important property reflecting the degree of structural safety [31]. The reliability-based optimization design measures the uncertainty of the structure by the failure probability or reliability index. While pursuing the optimal structural performance, it reduces the probability of the structure failure under the influence of uncertain factors, thereby improving the safety of the structure. Reliability-based topology optimization is a combination of reliability analysis and deterministic topology optimization design, aiming to integrate the problem of structural optimization and reliability constraint. The RBTO is slightly different from the traditional reliability structure optimization, and the variables are mainly divided into deterministic variables and random variables. The deterministic variables are used to characterize the physical density ρ (in the case of the variable density method), which are the design variable for topology optimization. And the random variables Y , which are used to characterize the structural uncertainty factor, are continuous variables. This paper mainly studies random uncertain variables, such as the material properties of structures, loads, etc., which are suitable for using probability theory to describe their distribution characteristics [32]. In order to facilitate the calculation, it is generally necessary to standardize the non-normally distributed random variables into mutually independent standard normal random variables u .

4.2. Mathematical Model of Reliability-Based Topology Optimization

Based on the above description of the random variables, a mathematical model for reliability-based topology optimization of thermo-elastic structure is established. Considering a general RBTO formulation, the stress constraint of Equation (8) is simply transformed into a probabilistic constraint, as follows

$$\begin{cases} \text{find } \boldsymbol{\rho} \\ \min V(\boldsymbol{\rho}) = \sum_{e=1}^{N_e} \rho_e v_e \\ \text{s.t. } P_r[G(\boldsymbol{\rho}, \mathbf{Y}) \leq 0] = P_f \leq P_f^* \\ P_f = \int_{G \leq 0} f_Y(\mathbf{y}) d\mathbf{y}_1 \cdots d\mathbf{y}_n \\ 0 < \rho_{\min} \leq \rho_e \leq 1 (e = 1, 2, \dots, N_e) \end{cases} \quad (20)$$

This optimization model is expressed as finding the optimized structural configuration, i.e., minimizing the overall structural volume under the reliability stress constraint. \mathbf{Y} is a vector of random variables, G is a limit state function, $f_Y(\mathbf{y})$ is the joint probability density function of \mathbf{Y} , P_r is the probability sign, P_f is the failure probability, obtained by multidimensional integration, and P_f^* is the value of the permissible failure probability. In reliability analysis, the limit state is defined as $G(\boldsymbol{\rho}, \mathbf{Y}) = 0$, the failure state and the safety state are $G(\boldsymbol{\rho}, \mathbf{Y}) < 0$ and $G(\boldsymbol{\rho}, \mathbf{Y}) > 0$, respectively.

In practical engineering, it is difficult to solve the multidimensional integral to obtain the exact probability density distribution. Therefore, approximate analytical methods are generally used to calculate the failure probability, such as the first order second moment method [33] and the first order reliability method [34]. The first order reliability method is selected in this paper to approximate the failure probability.

According to the stress intensity interference theory [35,36], this paper characterizes the limit state function, G , in terms of the load-bearing capacity of the structure, denoted as

$$G(\boldsymbol{\rho}, \mathbf{Y}) = R - S = \sigma_s - \sigma_e^{VM}(\boldsymbol{\rho}, \mathbf{Y}) \quad (21)$$

where R denotes the structural resistance and S denotes the load variable. In this paper, we consider the possibility that the random variables may cause the von Mises stress somewhere in the structure to exceed the yield strength limit of the material, thus causing the structure to fail. So here R is denoted as the yield strength σ_s of the material and S is denoted as the von Mises stress $\sigma_e^{VM}(\boldsymbol{\rho}, \mathbf{Y})$ of element. $G > 0$, the structure is reliable, $G < 0$, the structure fails, and $G = 0$, the structure is in the limit state.

If both R and S obey normal distribution, their mean and variance are φ_R , φ_S and σ_R , σ_S , respectively. Then G also obeys normal distribution, and let its mean and variance be φ_G and σ_G , respectively. Therefore, the failure probability can be expressed as

$$P_f = P_r[\sigma_s - \sigma_e^{VM}(\boldsymbol{\rho}, \mathbf{Y}) \leq 0] = \Phi\left(\frac{\varphi_S - \varphi_R}{(\sigma_R^2 + \sigma_S^2)^{1/2}}\right) = \Phi\left(-\frac{\varphi_G}{\sigma_G}\right) \quad (22)$$

where Φ is the standard cumulative distribution function.

Introducing the reliability index β , let be

$$\beta = \frac{\varphi_G}{\sigma_G} \quad (23)$$

Using the first order reliability method, the calculation of the probability of failure is converted into a measurable reliability index β , which is specifically expressed as the minimum distance from the origin to the limit state function in the normalized space (\mathbf{u} space) with the most probable point (MPP) being searched, as shown in Figure 2. According to the corresponding relationship of the failure probability and the reliability index in the first order reliability method, the failure probability constraint can be transformed into the following reliability index constraint

$$\begin{cases} P_f = \Phi(-\beta) \\ P_f^* = \Phi(-\beta^*) \\ P_f \leq P_f^* \Rightarrow \beta \geq \beta^* \end{cases} \tag{24}$$

where β^* is the target reliability index, and the intersection point \mathbf{u}^* is the design point, also known as the most probable failure point (MPP). The random variable Y needs to be normalized into an independent standard normal random variable \mathbf{u} , expressed as $\mathbf{u} = T(\mathbf{Y})$, or $\mathbf{Y} = T^{-1}(\mathbf{u})$. In the standard normal space, \mathbf{u} is given by the following expression, defined as

$$\mathbf{u} = \frac{\mathbf{Y} - \boldsymbol{\varphi}_y}{\boldsymbol{\sigma}_y} \tag{25}$$

where $\boldsymbol{\varphi}_y$ and $\boldsymbol{\sigma}_y$ are the vector of mean values and the standard deviations associated with Y , respectively.

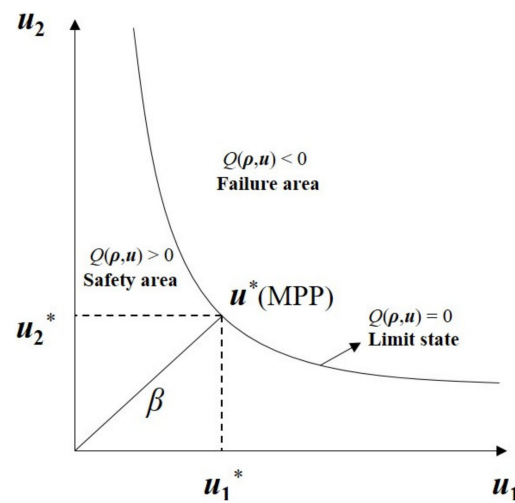


Figure 2. Geometric description of reliability index in standard normal space.

After the above transformation, in the standard normal space, the limit state function is then transformed into

$$G(\boldsymbol{\rho}, \mathbf{Y}) = G\left(\left(\boldsymbol{\rho}, T^{-1}(\mathbf{u})\right)\right) = Q(\boldsymbol{\rho}, \mathbf{u}) \tag{26}$$

4.3. Reliability-Based Topology Optimization for Thermo-Elastic Structures

The design variables and random variables in the reliability-based topology optimization are respectively assigned into deterministic topology optimization and reliability analysis and are independent of each other, which leads to the reliability-based topology optimization computation intensively and makes it difficult to converge [37]. Therefore, the proposed predecessor-decoupling hybrid method is adopted that decomposed the RBTO problem into two successively independent design processes that the deterministic topology optimization and reliability analysis.

In the reliability analysis, the MPP point \mathbf{u}^* is obtained by solving the following mathematical model according to the geometric meaning of the reliability index β in Figure 2.

$$\begin{cases} \min_{\mathbf{u}} \|\mathbf{u}\| = \beta = \sqrt{\sum u_i^2} \\ s.t. \beta(\mathbf{u}) \geq \beta^* \end{cases} \tag{27}$$

The sensitivity of the reliability index concerning the normal random variable can be expressed as

$$\frac{\partial \beta}{\partial u_i} = \frac{1}{2} \left(\sum u_i^2\right)^{-1/2} 2u_i = \frac{u_i}{\beta} \tag{28}$$

The sensitivity of the objective function with respect to the chosen means of random variables can simply be calculated using the classical finite difference approach, written as

$$\frac{\partial V}{\partial \varphi_{y_i}} = \frac{\Delta V}{\Delta \varphi_{y_i}} = \frac{V(\varphi_{y_i} + \Delta \varphi_{y_i}) - V(\varphi_{y_i})}{\Delta \varphi_{y_i}} \tag{29}$$

where φ_{y_i} and σ_{y_i} are the mean value and standard deviation of the random variable y_i , respectively.

According to the above sensitivity calculation result, the revised random variable y^* through Rosenblatt inverse transform, is defined as

$$\begin{cases} y_i^* = \varphi_{y_i} + u_i^* \sigma_{y_i}, & \frac{\partial V}{\partial \varphi_{y_i}} \geq 0 \\ y_i^* = \varphi_{y_i} - u_i^* \sigma_{y_i}, & \frac{\partial V}{\partial \varphi_{y_i}} \leq 0 \end{cases} \tag{30}$$

5. Sensitivity Analysis

The sensitivity of the structural volume respect to the element density can be obtained by the direct differentiation method, defined by

$$\frac{\partial V(\rho)}{\partial \rho_e} = v_0 \tag{31}$$

The sensitivity information of the stress relative to the element density is obtained by the adjoint variable method. The Lagrangian function C of the stress is constructed by introducing the Lagrangian product factor as

$$C = \bar{\sigma}^{PN} - \lambda^T \left(\mathbf{K}(\rho) \mathbf{U} - \mathbf{F}^m - \mathbf{F}^{th}(\rho) \right) \tag{32}$$

The sensitivity of the Lagrangian function with respect to the element density is derived as

$$\frac{\partial C}{\partial \rho_e} = \frac{\partial \bar{\sigma}^{PN}}{\partial \rho_e} - \lambda^T \left(\frac{\partial \mathbf{K}(\rho)}{\partial \rho_e} \mathbf{U} + \mathbf{K}(\rho) \frac{\partial \mathbf{U}}{\partial \rho_e} - \frac{\partial \mathbf{F}^m}{\partial \rho_e} - \frac{\partial \mathbf{F}^{th}(\rho)}{\partial \rho_e} \right) \tag{33}$$

According to the chain rule, it is easy to obtain the sensitivity corresponding the element density ρ_e as

$$\frac{\partial \bar{\sigma}^{PN}}{\partial \rho_e} = \sum_{i=1}^{N_e} c \frac{\partial \bar{\sigma}^{PN}}{\partial \sigma_e^{VM}} \left(\frac{\partial \sigma_e^{VM}}{\partial \rho_e} \right)^T \frac{\partial \sigma_e}{\partial \rho_e} \tag{34}$$

From the above equation, the sensitivity information for solving the global stress can be obtained by combining the derivative of the p-norm function with respect to the von Mises stress, the derivative of the von Mises stress with respect to the stress component, and the derivative of the stress component with respect to the design variable. This sensitivity information is performed separately.

5.1. Derivative of the p-Norm Function with Respect to the Von Mises Stress

Taking the expression of Equation (16), the derivative information of the p-norm function to the von Mises stress of each element can be obtained as

$$\frac{\partial \bar{\sigma}^{PN}}{\partial \sigma_e^{VM}} = \left(\sum_{e=1}^{N_e} \left(\frac{\sigma_e^{VM}}{\sigma_s} \right)^p \right)^{\frac{1}{p}-1} \left(\frac{\sigma_e^{VM}}{\sigma_s} \right)^{p-1} \frac{1}{\sigma_s} \tag{35}$$

5.2. Derivative of the Von Mises Stress with Respect to the Stress Component

For planar and spatial structural problems, the derivatives of element stress with respect to the stress components are respectively described as

For 2D problems,

$$\begin{cases} \frac{\partial \sigma_e^{VM}}{\partial \sigma_{ex}} = \frac{1}{2\sigma_e^{VM}} (2\sigma_{ex} - \sigma_{ey}) \\ \frac{\partial \sigma_e^{VM}}{\partial \sigma_{ey}} = \frac{1}{2\sigma_e^{VM}} (2\sigma_{ey} - \sigma_{ex}) \\ \frac{\partial \sigma_e^{VM}}{\partial \tau_{exy}} = \frac{3\tau_{exy}}{\sigma_e^{VM}} \end{cases} \quad (36)$$

For 3D problems,

$$\begin{cases} \frac{\partial \sigma_e^{VM}}{\partial \sigma_{ex}} = \frac{1}{2\sigma_e^{VM}} (2\sigma_{ex} - \sigma_{ey} - \sigma_{ez}) \\ \frac{\partial \sigma_e^{VM}}{\partial \sigma_{ey}} = \frac{1}{2\sigma_e^{VM}} (2\sigma_{ey} - \sigma_{ex} - \sigma_{ez}) \\ \frac{\partial \sigma_e^{VM}}{\partial \sigma_{ez}} = \frac{1}{2\sigma_e^{VM}} (2\sigma_{ez} - \sigma_{ex} - \sigma_{ey}) \\ \frac{\partial \sigma_e^{VM}}{\partial \tau_{exy}} = \frac{3\tau_{exy}}{\sigma_e^{VM}} \\ \frac{\partial \sigma_e^{VM}}{\partial \tau_{exz}} = \frac{3\tau_{exz}}{\sigma_e^{VM}} \\ \frac{\partial \sigma_e^{VM}}{\partial \tau_{ezx}} = \frac{3\tau_{ezx}}{\sigma_e^{VM}} \end{cases} \quad (37)$$

5.3. Derivative of Stress Components with Respect to Design Variable

The derivative of the element stress component with respect to the density variable is obtained as

$$\frac{\partial \sigma_e}{\partial \rho_e} = q\rho_e^{q-1} E_0 (\mathbf{D}_0 \mathbf{B}_e \mathbf{U}_e - \mathbf{D}_0 \gamma_0 \phi \Delta T) + \rho_e^q E_0 \mathbf{D}_0 \mathbf{B}_e \frac{\partial \mathbf{U}_e}{\partial \mathbf{U}} \frac{\partial \mathbf{U}_e}{\partial \rho_e} \quad (38)$$

Considering the loading independence, the derivative of the mechanical load \mathbf{F}^m on the element density can be ignored, and combining Equation (35) with Equation (34) and substituting it into Equation (33), we can obtain

$$\begin{aligned} \frac{\partial \mathbf{C}}{\partial \rho_e} &= \sum_{e=1}^{N_e} c \frac{\partial \sigma^{PN}}{\partial \sigma_e^{VM}} \left(\frac{\partial \sigma_e^{VM}}{\partial \sigma_e} \right)^T q\rho_e^{q-1} E_0 (\mathbf{D}_0 \mathbf{B}_e \mathbf{U}_e - \mathbf{D}_0 \gamma_0 \phi \Delta T) \\ &\quad - \lambda^T \left(\frac{\partial \mathbf{K}(\rho)}{\partial \rho_e} \mathbf{U} - \frac{\partial \mathbf{F}^{th}(\rho)}{\partial \rho_e} \right) \\ &\quad + \left[\sum_{e=1}^{N_e} c \frac{\partial \sigma^{PN}}{\partial \sigma_e^{VM}} \left(\frac{\partial \sigma_e^{VM}}{\partial \sigma_e} \right)^T \rho_e^q E_0 \mathbf{D}_0 \mathbf{B}_e \frac{\partial \mathbf{U}_e}{\partial \mathbf{U}} - \lambda^T \mathbf{K}(\rho) \right] \frac{\partial \mathbf{U}_e}{\partial \rho_e} \end{aligned} \quad (39)$$

In order to eliminate the unknown displacement sensitivity term, let the term containing $\partial \mathbf{U} / \partial \rho_e$ be zero, then the adjoint vector equation is established as

$$\mathbf{K}(\rho) \lambda = \sum_{e=1}^{N_e} c \frac{\partial \sigma^{PN}}{\partial \sigma_e^{VM}} \rho_e^q E_0 \left(\frac{\partial \mathbf{U}_e}{\partial \mathbf{U}} \right)^T \mathbf{B}_e^T \mathbf{D}_0^T \left(\frac{\partial \sigma_e^{VM}}{\partial \sigma_e} \right) \quad (40)$$

Then the corresponding sensitivity is

$$\begin{aligned} \frac{\partial \mathbf{C}}{\partial \rho_e} &= \sum_{e=1}^{N_e} c \frac{\partial \sigma^{PN}}{\partial \sigma_e^{VM}} \left(\frac{\partial \sigma_e^{VM}}{\partial \sigma_e} \right)^T q\rho_e^{q-1} E_0 q\rho_e^{q-1} E_0 (\mathbf{D}_0 \mathbf{B}_e \mathbf{U}_e - \mathbf{D}_0 \gamma_0 \phi \Delta T) \\ &\quad - \lambda^T \left(\frac{\partial \mathbf{K}(\rho)}{\partial \rho_e} \mathbf{U} - \frac{\partial \mathbf{F}^{th}(\rho)}{\partial \rho_e} \right) \end{aligned} \quad (41)$$

Combining Equation (4) information, the derivation of Equations (2) and (7) can respectively obtain the sensitivity of stiffness matrix $\mathbf{K}(\rho)$ and temperature load vector $\mathbf{F}^{th}(\rho)$, defined as

$$\frac{\partial \mathbf{K}(\rho)}{\partial \rho_e} = \sum_{e=1}^{N_e} \alpha \rho_e^{\alpha-1} E_0 \int_{\Omega_e} \mathbf{B}_e^T \mathbf{D}_0 \mathbf{B}_e h d\Omega_e \quad (42)$$

$$\frac{\partial F^{th}(\rho)}{\partial \rho_e} = \sum_{e=1}^{N_e} k \rho_e^{k-1} \delta_0 \Delta T \int_{\Omega_e} \mathbf{B}_e^T \mathbf{D}_0 \boldsymbol{\phi} d\Omega_e \tag{43}$$

6. Density Filtering

In order to avoid the phenomenon of checkerboard and intermediate elements in the topology optimization results, the density filtering technology [38] is used to suppress the problems that are defined as

$$\rho_e = \frac{1}{\sum_{i \in N_e} H_{ei}} \sum_{i \in N_e} H_{ei} x_i \tag{44}$$

where ρ_e is the element density, which is used to calculate the volume and stiffness matrix of the element, x_i is the design variable of the element, N_e is the number of all elements whose distance from the center of element e is less than the filter radius r_{min} , and H_{ei} is the linear distance function, namely

$$H_{ei} = \max(0, r_{min} - \Delta(e, i)) \tag{45}$$

where $\Delta(e, i)$ is the distance between the centers of element e and element i .

The difference between the design variable x and the physical density ρ can be noted here. The finite element model is parameterized using the density variable ρ_e contained in ρ . The density variable is now calculated by applying a density filter to the design variable x . For sensitivity consistency, the following chain rule is used, where g is the objective or constraint function

$$\frac{\partial g}{\partial x_j} = \sum_{e \in N_j} \frac{\partial g}{\partial \rho_e} \frac{\partial \rho_e}{\partial x_j} = \sum_{e \in N_j} \frac{1}{\sum_{i \in N_e} H_{ei}} H_{je} \frac{\partial g}{\partial \rho_e} \tag{46}$$

The method of moving asymptote (MMA) [39] is used to solve the reliability-based stress-constrained topology optimization problem for thermo-elastic structures. Due to the highly nonlinear behavior of the stress constraint, the optimization process is prone to iterative oscillations and even non-convergence. To avoid non-convergence, then an external move limit m is imposed on the MMA algorithm to limit the maximum absolute value of the difference between the design variables updated during the current iteration and the previous iteration step.

In summary, the design of the reliability topology optimization of thermo-elastic structures considering the stress constraint based on the hybrid precursor-decoupling format is decoupled into two parts executed in separate sequences: the precursor reliability analysis and the deterministic topology optimization. The specific process is: first, according to the geometric meaning of the reliability index in the primary reliability method, seek the design point that satisfies the target reliability index; then, according to the sensitivity information of the random variable, modify the random variable and convert it into a deterministic parameter; finally, the deterministic topology optimization design is carried out. The specific optimization flowchart is shown in Figure 3.

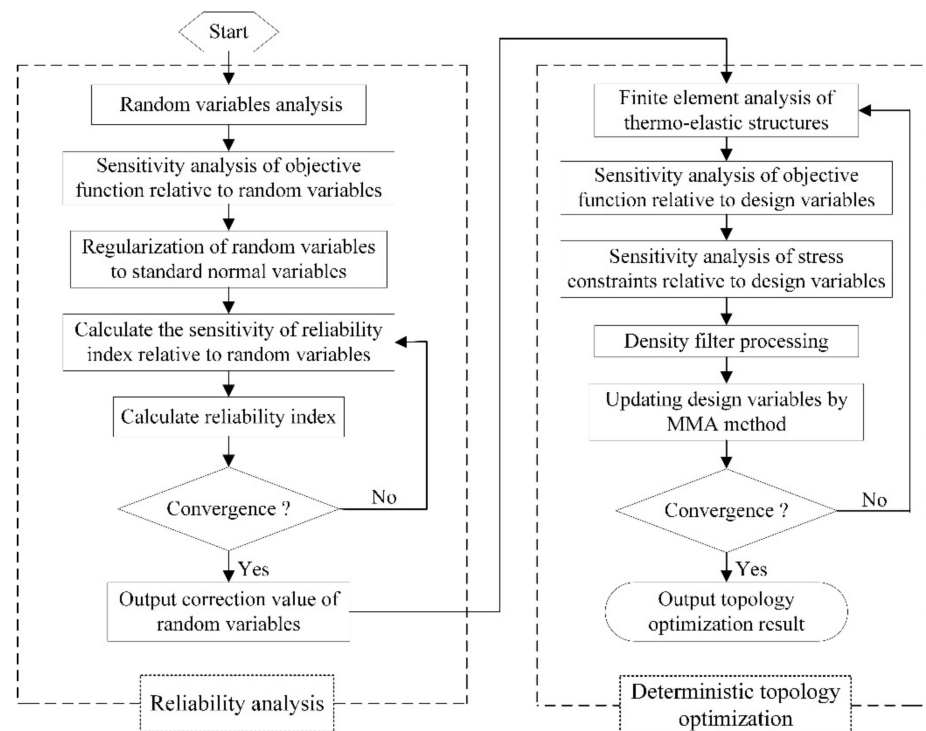


Figure 3. Flowchart of reliability topology optimization in hybrid format.

7. Numerical Examples

In this section, three numerical examples of reliability-based stress-constrained topology optimization of thermo-elastic structures are selected to verify the effectiveness of the proposed method. The selected materials are chosen with the Young’s modulus $E = 2.1 \times 10^5$ MPa, Poisson’s ratio $\mu = 0.3$, thermal expansion coefficient $\gamma_0 = 12.1 \times 10^{-6}/^\circ\text{C}$. The p-norm penalization factor is $p = 8$. The penalty factors are defined as $\alpha = 3$, $k = 3$, and $q = 0.8$. The initial element density values are taken as 1. The corresponding initial design domain volume is V_0 , and the ratio V/V_0 of the optimized structure volume to the initial structure volume is used as the objective function, and the temperature field is uniformly varying.

7.1. 2D L-Shaped Beam Structure

The design domain of the L-shaped beam structure is illustrated in Figure 4. The design domain has dimensions of $120 \text{ mm} \times 120 \text{ mm}$ with a thickness of 1 mm and is discretized into 14,400 quadrilateral elements. The top end of the L-shaped beam structure is clamped and the mechanical load F^m is applied to the upper right end of the structure, which is uniformly distributed over six adjacent nodes to avoid stress concentration. The stress constraint value for the structure is 235 MPa, and the amount of temperature change $\Delta T = 10^\circ\text{C}$.

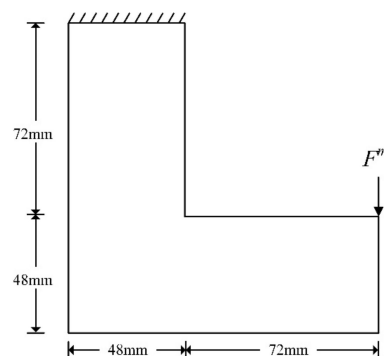


Figure 4. Design domain of L-shaped beam.

For the reliability analysis, the random variables are chosen as $Y = (F^m, E, \delta_0)^T$, and assume that they obey normal probabilistic distribution. The mean value of mechanical load, Young’s modulus and thermal stress coefficient are $\varphi_{F^m} = 280 \text{ N}$, $\varphi_E = 2.1 \times 10^5 \text{ MPa}$ and $\varphi_{\delta_0} = 2.541 \text{ MPa}/^\circ\text{C}$, respectively. The variance is set to 5% of the mean value and the permitted reliability index is set to 3.0.

The detailed evolution of the deterministic and reliable structures and the von Mises stress distribution are shown in Figures 5 and 6, respectively, and the initial structural maximum on the von Mises stress value is 246.82 MPa. The optimized deterministic and reliable topological configurations and von Mises stress distributions are shown in Figures 7 and 8, respectively. The corresponding topology optimization results are shown in Table 1, and the reliability indexes are calculated using the Monte Carlo simulation method, where u_1, u_2 , and u_3 correspond to the standard normalized variable values of the random variables F^m, E , and δ_0 , respectively.

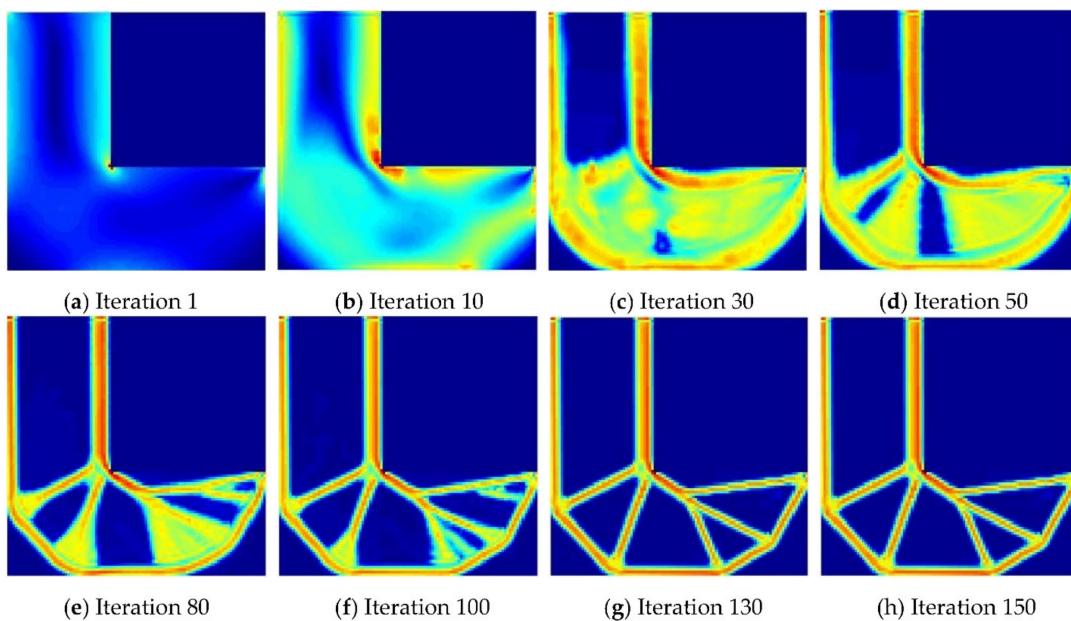


Figure 5. Structural evolution for deterministic topology optimization with stress distribution (a–h).

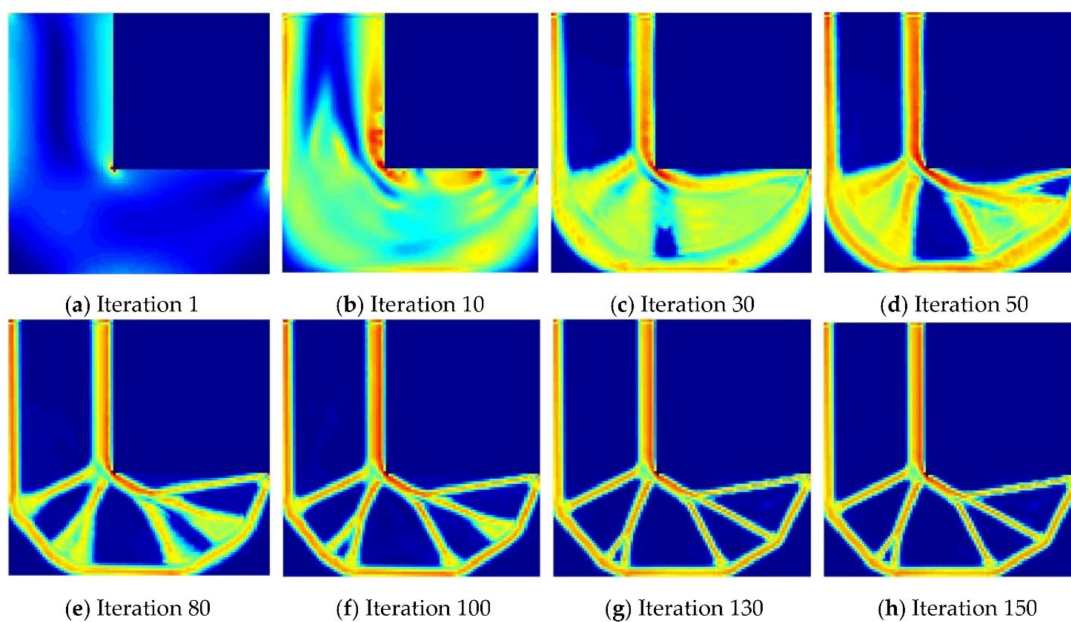


Figure 6. Structural evolution for reliability topology optimization with stress distribution (a–h).

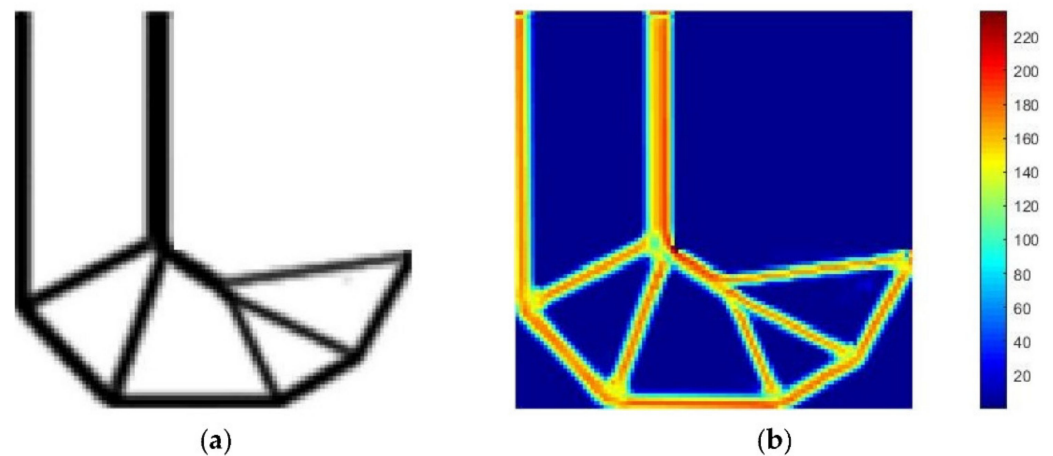


Figure 7. Deterministic topology optimization result of L-beam structure (14,400 elements): (a) Topological structure; (b) Von Mises stress distribution.

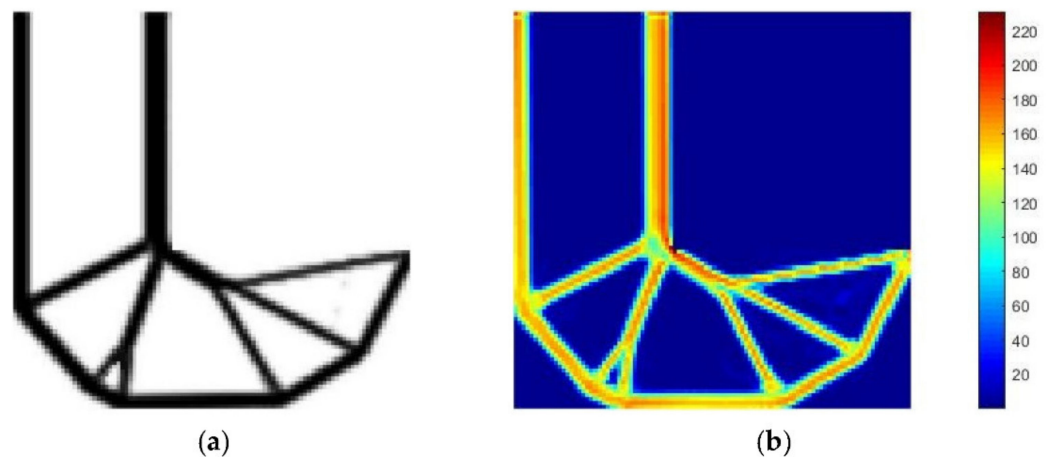


Figure 8. Reliability topology optimization result of L-beam structure (14,400 elements): (a) Topological structure; (b) Von Mises stress distribution.

Table 1. Comparison of topology optimization design results.

| Approach | Volume Fraction (%) | Reliability Index (β) | Computing Time (s) | Max Von Mises Stress (MPa) | MPP (u_1, u_2, u_3) |
|----------|---------------------|-------------------------------|--------------------|----------------------------|--------------------------|
| DTO | 19.8 | 1.7759×10^{-5} | 371.63 | 234.95 | - |
| RBTO | 24.3 | 2.9745 | 395.49 | 234.60 | (1.7321, 1.7321, 1.7321) |

In addition, in order to illustrate that the number of elements in the divided design domain has no obvious effect on the optimized topology, the design domain shown in Figure 4 is discretized into 6400 quadrilateral elements, where the mechanical load F^m does not change, and is applied to the upper right end of the structure and uniformly distributed over four adjacent nodes. The optimized deterministic and reliable topologies and von Mises stress distributions are shown in Figures 9 and 10, respectively.

By observing Figures 5 and 6 and Table 1, it can be seen that the right-angle corner of the initial structure is the stress concentration area, and the maximum von Mises stress exceeds the material strength. The structure after deterministic and reliable topology optimization not only reduces the maximum von Mises stress, but also meets the strength requirements of the material, and the original stress concentration corner evolves into a rounded structure, which alleviates the stress concentration phenomenon.

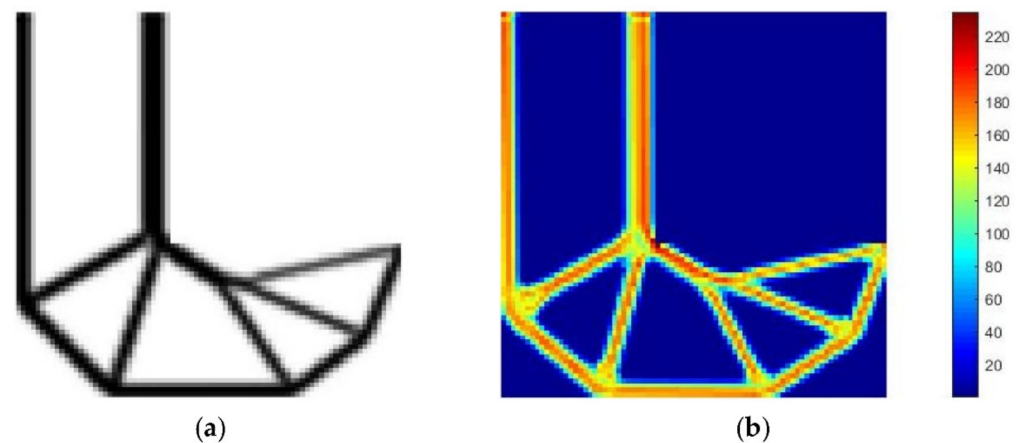


Figure 9. Deterministic topology optimization result of L-beam structure (6400 elements): (a) Topological structure; (b) Von Mises stress distribution.

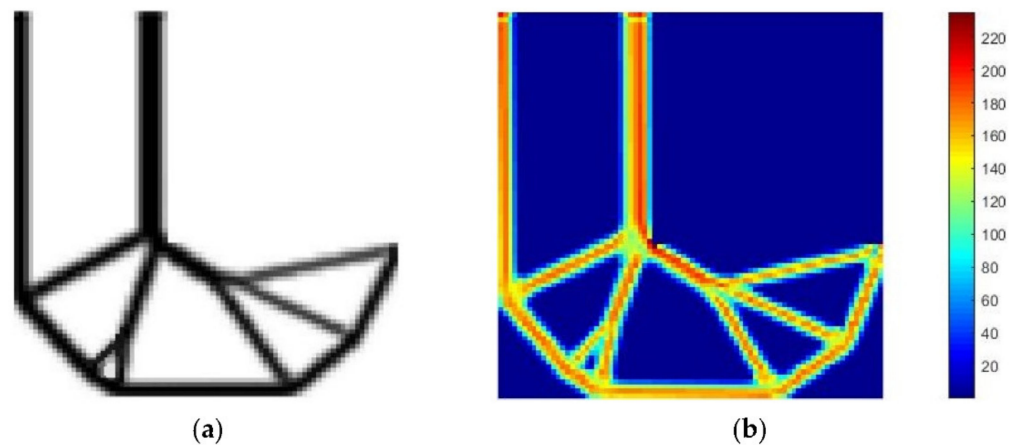


Figure 10. Reliability topology optimization result of L-beam structure (6400 elements): (a) Topological structure; (b) Von Mises stress distribution.

The results for DTO and RBTO show very different optimal topologies, where DTO is less reliable and therefore allows less margin for performance fluctuations and an increased probability of structural failure when parameter variations that are considered as random variables are considered. The topology obtained from RBTO uses about 4% more material than DTO to make the structure meet the target reliability index. We also find that RBTO obtains a slightly lower computational efficiency due to the need to solve the MPP in the reliability analysis. In terms of the respective stress distribution, the RBTO presents a more uniform stress distribution in the structure compared to the DTO, and the structure is subjected to a smaller maximum von Mises stress value. Finally, comparing the topological configurations in Figures 7 and 8 with Figures 9 and 10, respectively, it can be seen that the deterministic and reliable topological configurations under different numbers of elements are relatively similar, which indicates that the number of elements does not have a significant effect on the topological configuration, that is, the proposed method is mesh independence.

The volume fraction and maximum von Mises stress iteration curves for the DTO and RBTO processes shown in Figures 7 and 8 are shown in Figure 11. The results show that the iterative oscillation of the maximum von Mises stress during optimization is caused by the highly nonlinear behavior of the stress constraint. Compared with DTO, the fluctuation degree of the maximum von Mises stress in the iterative process of RBTO is reduced, and the iterative process is more stable. The above analysis can show that the proposed method is feasible and effective.

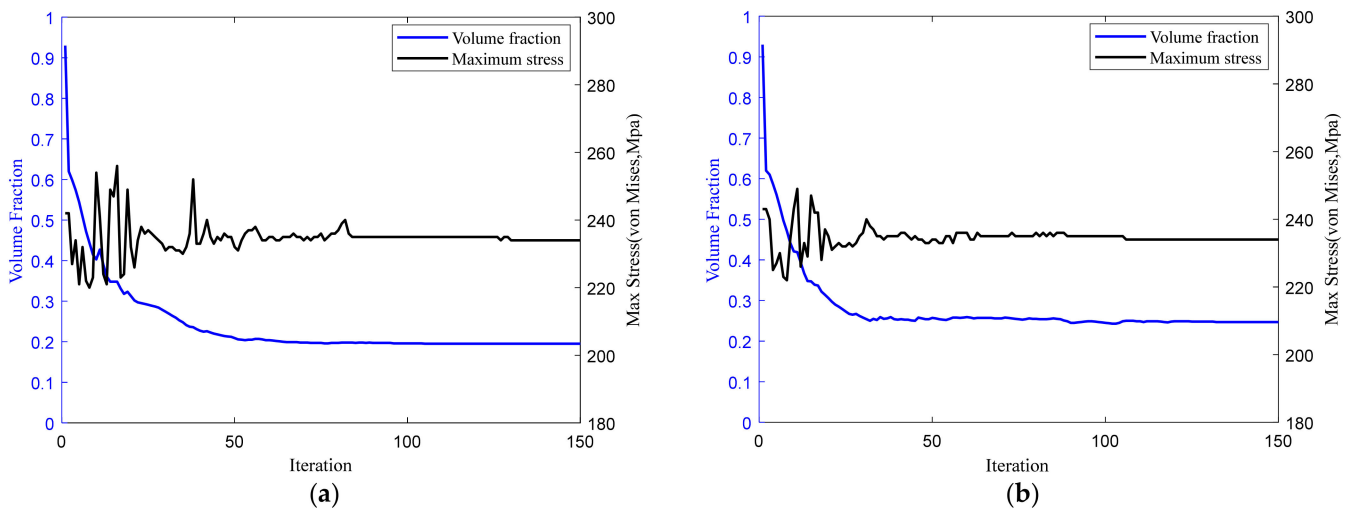


Figure 11. Volume fraction and maximum von Mises stress iteration curves of (a) DTO and (b) RBTO.

7.2. 2D T-Shaped Beam Structure

The design domain of the T-beam structure is shown in Figure 12. The design domain is 160 mm × 100 mm in structural dimensions and 1 mm in thickness, which is discretized into 16,000 four-node elements. The left and right sides of the structure are solidly supported, and the mechanical loads F_x^m and F_y^m are applied to the upper right end of the structure, which are uniformly distributed to the five adjacent nodes horizontally. The stress constraint value for the structure is 235 MPa.

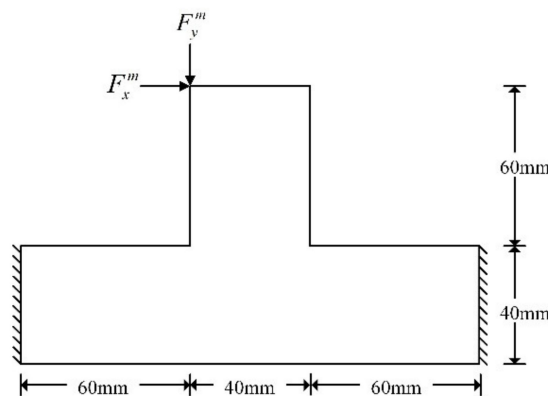


Figure 12. Design domain of T-shaped beam.

For the reliability analysis, the random variables are chosen as $Y = (F_x^m, F_y^m, E, \delta_0)^T$, and assume that they obey normal probabilistic distribution. The mean value of mechanical loads, Young’s modulus and thermal stress coefficient are $\varphi_{F_x^m} = 350$ N, $\varphi_{F_y^m} = 300$ N, $\varphi_E = 2.1 \times 10^5$ MPa and $\varphi_{\delta_0} = 2.541$ MPa/°C, respectively. The variance is set to 10% of the mean value.

The initial stress distribution of the structure is shown in Figure 13, and the maximum von Mises stress value is 315.04 MPa. In order to consider the effect of different temperature variations ΔT on the topology optimization results, when the temperature variations ΔT are set to 20 °C and 30 °C, the DTO and RBTO topologies and von Mises stress distributions obtained are shown in Figures 14 and 15, respectively. The corresponding topology optimization results are shown in Table 2, and the reliability indexes are calculated using the Monte Carlo simulation method, where u_1, u_2, u_3 and u_4 correspond to the standard normalized variable values of the random variables F_x^m, F_y^m, E and δ_0 , respectively.

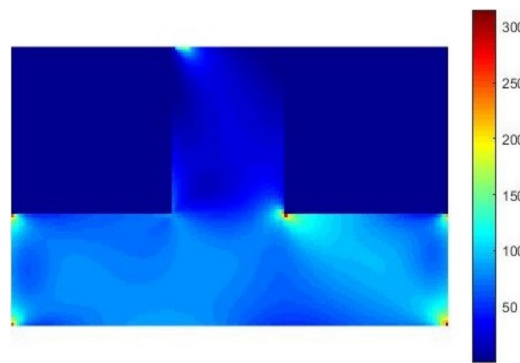


Figure 13. Initial structural stress distribution.

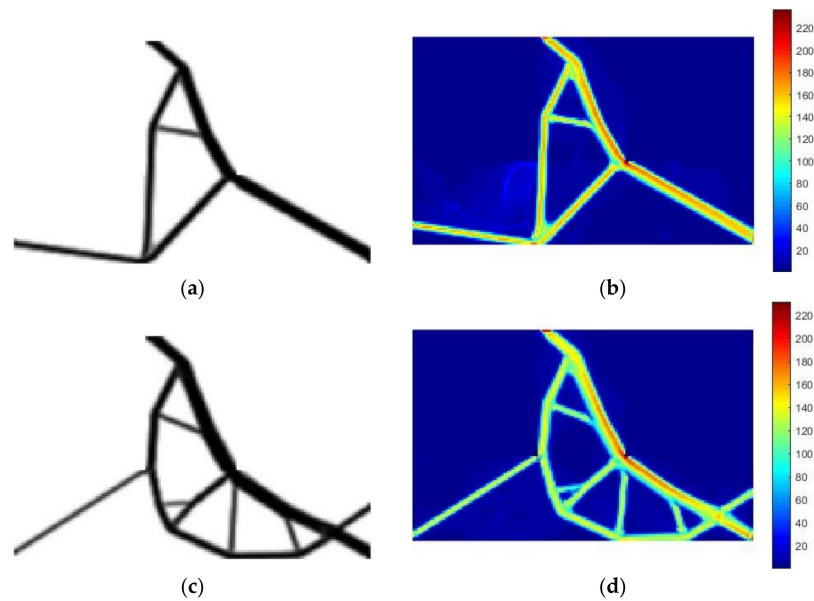


Figure 14. Topology optimization results of T-beam ($\Delta T = 20\text{ }^{\circ}\text{C}$): (a) DTO topological structure (b) DTO Von Mises stress distribution; (c) RBTO topological structure; (d) RBTO Von Mises stress distribution.

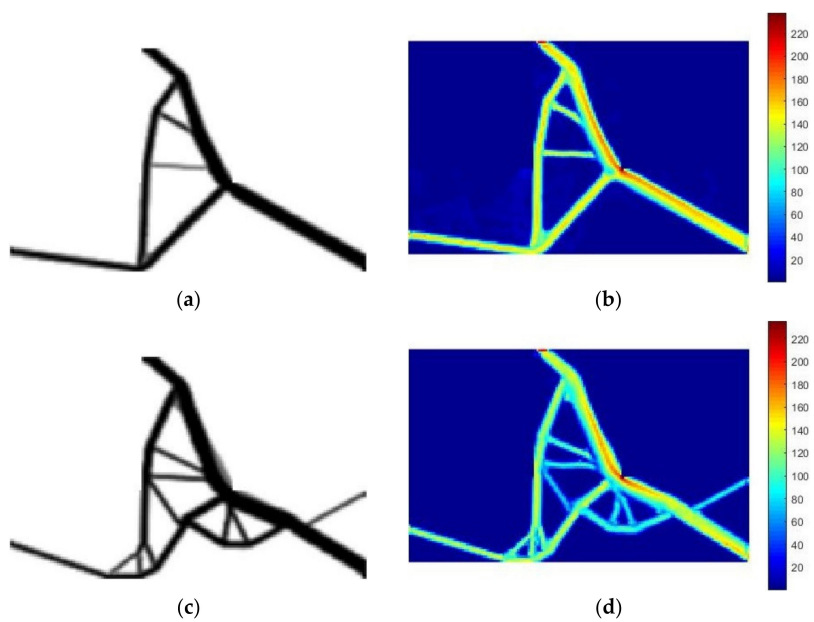


Figure 15. Topology optimization results of T-beam ($\Delta T = 30\text{ }^{\circ}\text{C}$): (a) DTO topological structure; (b) DTO Von Mises stress distribution; (c) RBTO topological structure; (d) RBTO Von Mises stress distribution.

Table 2. Comparison of topology optimization design results.

| ΔT ($^{\circ}\text{C}$) | Approach | Volume Fraction (%) | Reliability Index (β) | Computing Time (s) | Max Von Mises Stress (MPa) | MPP (u_1, u_2, u_3, u_4) |
|-----------------------------------|----------|---------------------|-------------------------------|--------------------|----------------------------|------------------------------|
| 20 | DTO | 10.2 | 2.0201×10^{-5} | 354.02 | 234.96 | - |
| | RBTO | 13.5 | 3.9722 | 428.21 | 234.72 | (2.000, 2.000, 2.000, 2.000) |
| 30 | DTO | 11.2 | 2.5426×10^{-5} | 359.37 | 234.85 | - |
| | RBTO | 14.4 | 3.9764 | 435.19 | 234.53 | (2.000, 2.000, 2.000, 2.000) |

By comparing the above optimization results with the initial structure, it can be seen that the right-angle part of the original structure evolves into a slightly rounded shape, which relieves the stress concentration, the stress distribution of the structure is uniform, and the design results of both DTO and RBTO meet the stress constraint requirements.

Comparing the reliability indicators of DTO and RBTO results in Table 2, we can see that the reliability level of the DTO results is close to 0, so the probability of structural failure is higher. The reliability index of RBTO results has been improved compared with that of the DTO results, but the target reliability has not been achieved precisely, and it also reflects that the proposed method can effectively improve the reliability of the structure, but the computational accuracy is still slightly inadequate. Compared with DTO, the structures obtained by RBTO are both significantly different, and the reliability of the structure is improved, and the overall stress distribution of the structures is more uniform.

A comparative analysis of the optimization results of the structures in Table 2 shows that the topologies of both DTO and RBTO are slightly different for different temperature variations ΔT . This is mainly due to the fact that as the temperature variation ΔT increases, the temperature load enlarges and more material needs to be filled to bring the structures to the allowed reliability index, which leads to a slight increase in volume.

The volume fraction and maximum von Mises stress iteration curves for the DTO and RBTO at different temperature variations ΔT are shown in Figure 16, respectively. Compared with DTO, RBTO has less fluctuation of the maximum von Mises stress during the iterative process. It can be demonstrated that it is necessary and effective to incorporate the reliability analysis into the stress-constrained topology optimization of a thermo-elastic problem considering the uncertainties of mechanical loads, the thermal stress coefficient, and the material’s property.

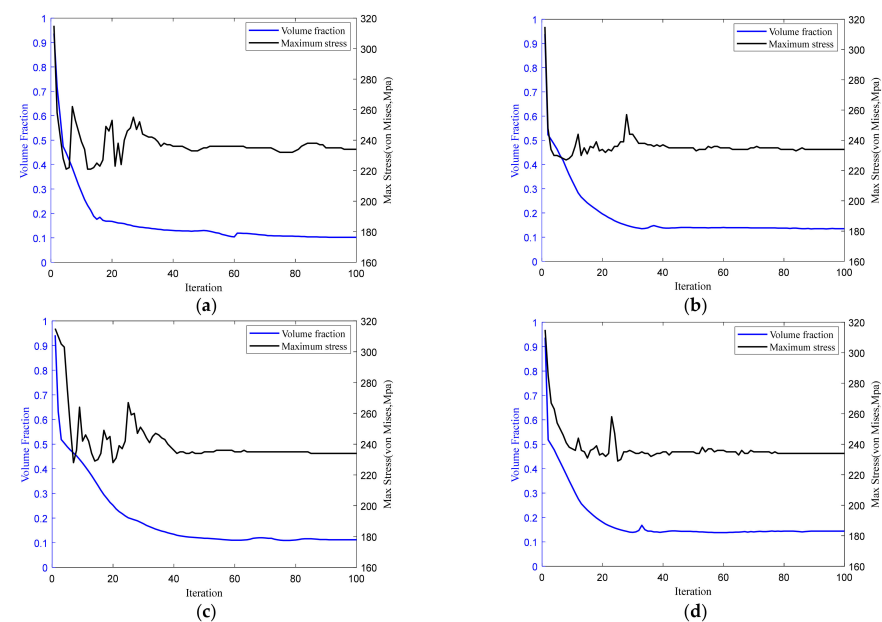


Figure 16. Volume fraction and maximum von Mises stress iteration curves of (a) DTO ($\Delta T = 20^{\circ}\text{C}$) and (b) RBTO ($\Delta T = 20^{\circ}\text{C}$); (c) DTO ($\Delta T = 30^{\circ}\text{C}$) and (d) RBTO ($\Delta T = 30^{\circ}\text{C}$).

7.3. 3D L-Shaped Beam Structure

In this section, we extend the previous 2D L-bracket example to a 3D design problem. The design domain of the 3D L-beam structure is shown in Figure 17. The design domain size is 50 mm \times 50 mm and the thickness is 4 mm. The domain is discrete into 10,000 eight-node hexahedral elements. The upper left of the structure is fixed. The mechanical load F^m is applied vertically downward on the right side of the structure. The stress constraint value for the structure is 235 MPa and the amount of temperature change $\Delta T = 30$ $^{\circ}\text{C}$.

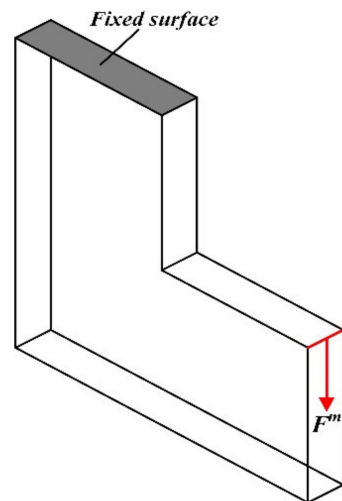


Figure 17. 3D L-beam design domain.

For the reliability analysis, the random variables are chosen as $Y = (F^m, E, \delta_0)^T$ and assume that they obey normal probabilistic distributions. The mean values of mechanical load, Young's modulus and thermal stress coefficient are $\varphi_{F^m} = 67$ N, $\varphi_E = 2.1 \times 10^5$ MPa and $\varphi_{\delta_0} = 2.541$ MPa/ $^{\circ}\text{C}$, respectively. The variance is set to 7% of the mean value, and the permissible reliability index is set to 5.0.

The initial structural stress distribution is shown in Figure 18 and the maximum von Mises stress value is 273.81 MPa. The deterministic and reliable topologies and von Mises stress distributions are shown in Figures 19 and 20, respectively. The corresponding topology optimization results are shown in Table 3, and the reliability indexes are calculated using the Monte Carlo simulation method, where u_1 , u_2 , and u_3 correspond to the standard normalized variable values of the random variables F^m , E , and δ_0 , respectively.

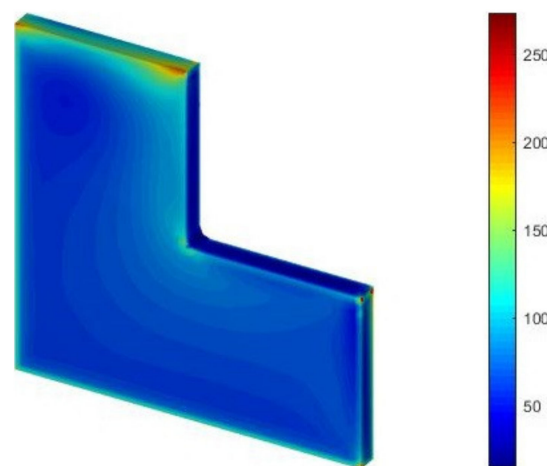


Figure 18. Initial structural stress distribution.

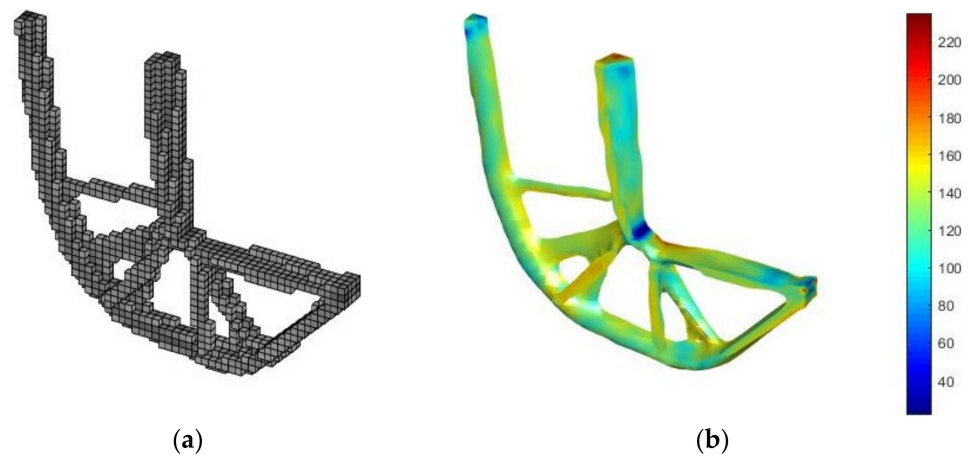


Figure 19. Deterministic topology optimization results for 3D L-shaped beam: (a) Topological structure; (b) Von Mises stress distribution.

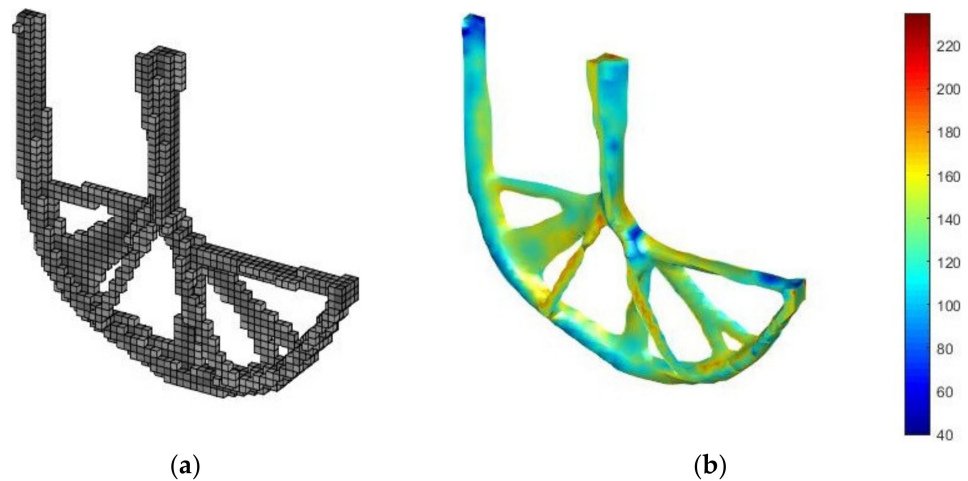


Figure 20. Reliability topology optimization results for 3D L-shaped beam: (a) Topological structure; (b) Von Mises stress distribution.

Table 3. Comparison of topology optimization design results.

| Approach | Volume Fraction (%) | Reliability Index (β) | Computing Time (s) | Max Von Mises Stress (MPa) | MPP (u_1, u_2, u_3) |
|----------|---------------------|-------------------------------|--------------------|----------------------------|--------------------------|
| DTO | 12.8 | 4.2818×10^{-5} | 326.02 | 234.93 | - |
| RBTO | 15.7 | 4.9864 | 383.62 | 234.65 | (2.8868, 2.8868, 2.8868) |

From the above optimization results, it can be seen that the DTO and RBTO optimal configurations also achieve the maximum von Mises stress constraint.

The analysis of the DTO and RBTO results show that the DTO result has a lower reliability level and a higher probability of structural failure. Similar to the 2D L-shaped problem, the structure obtained by RBTO has a significant difference compared to the DTO result, mainly in the filling of the lower part of the structure with bar material that increases the structural volume. In terms of stress distribution, the structure obtained by RBTO has more uniform stress distribution than that obtained by DTO, and the structure is more reliable and stable.

The volume fraction and maximum von Mises stress iteration curves of DTO and RBTO are shown in Figure 21, respectively. This 3D example proves that the reliability-based stress-constrained topology optimization method for thermo-elastic structures proposed in this paper is also applicable to the 3D structures problem, which has practical significance and application prospects for solving the uncertainty problem of thermo-elastic structures.

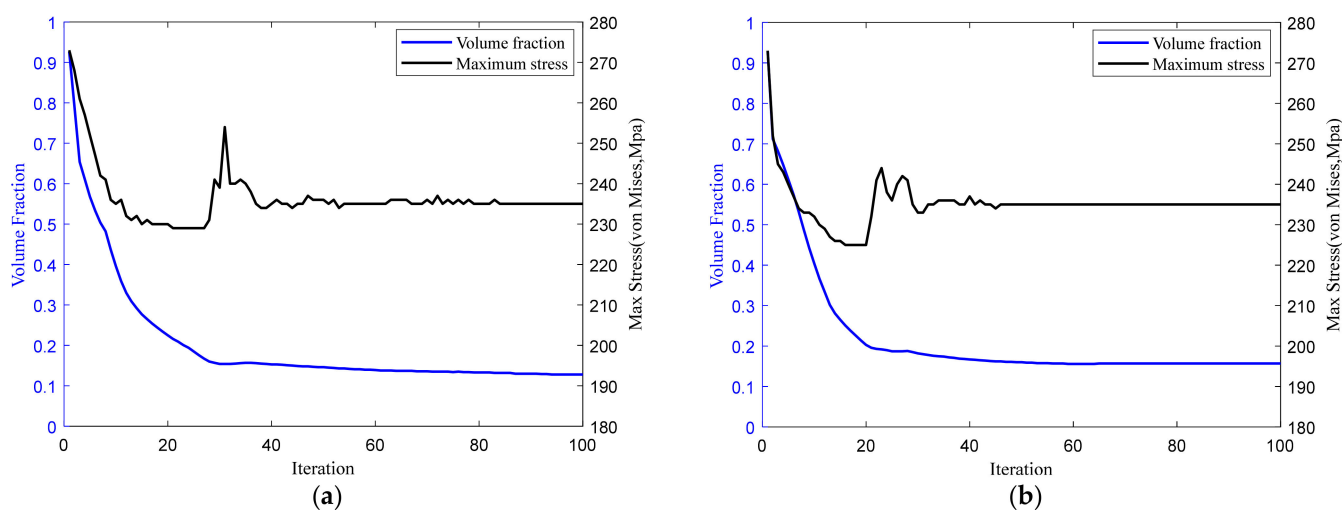


Figure 21. Volume fraction and maximum von Mises stress iteration curves of (a) DTO and (b) RBTO.

8. Conclusions

In this paper, the reliability analysis is integrated into SIMP-based topology optimization to solve the uncertainty problem in the stress-constraint topology optimization of thermo-elastic structures. The thermo-elastic topology optimization model based on global stress constraint considering the combined effect of temperature and mechanical load is established. The material property, the mechanical load and thermal stress coefficient are considered as uncertainty variables. Combining the deterministic topology optimization with the reliability hybrid method, the following conclusions can be drawn.

The structures after DTO and RBTO can satisfy the stress constraints, and the stress concentration phenomenon is alleviated. They differ in that the optimal topology obtained by the proposed RBTO method is more reliable than that obtained by the DTO method, and the RBTO exhibits significantly different topologies.

The corresponding DTO and RBTO results are also distinct for different temperature variations. It is also noted that as the temperature change increases, more material needs to be filled to meet the stress constraint and to reach the allowable reliability requirement.

The feasibility and effectiveness of the proposed method is verified by the 3D numerical example. It is shown that it is necessary to consider the uncertainty of the mechanical loads and material properties, thermal stress coefficients, and to incorporate the reliability concept into topology optimization.

In addition, the results of the above numerical examples show that the RBTO method in the predecessor-decoupling hybrid format used in this paper does not consider the influence of the functional function in the reliability analysis, so the calculation accuracy is slightly deficient. Therefore, further development of this work can try to introduce different reliability topology optimization methods for thermo-elastic structures with non-uniform temperature distribution for discussion to reduce the limitations.

Author Contributions: Formal analysis, L.Z.; funding acquisition, Q.Z.; supervision, Q.Z. and J.C.; data curation, L.Z.; writing—original draft preparation, L.Z.; writing—review and editing, Q.Z. and J.C. All authors have read and agreed to the published version of the manuscript.

Funding: The work described in this paper was supported by the National Natural Science Foundation of China (52175236).

Institutional Review Board Statement: Not applicable.

Informed Consent Statement: Not applicable.

Data Availability Statement: Not applicable.

Acknowledgments: The authors are thankful for Krister Svanberg for MMA program made freely available for research purposes and the anonymous reviewers for their helpful and constructive comments.

Conflicts of Interest: The authors declare that they have no conflict of interest.

References

1. Pedersen, P.; Pedersen, N.L. Interpolation/penalization applied for strength design of 3D thermo-elastic structures. *Struct. Multidiscip. Optim.* **2012**, *45*, 773–786. [[CrossRef](#)]
2. Rodrigues, H.; Fernandes, P. A material based model for topology optimization of thermo-elastic structures. *Int. J. Numer. Methods Eng.* **1995**, *38*, 1951–1965. [[CrossRef](#)]
3. Du, Y.X.; Luo, Z.; Tian, Q.H.; Chen, L.P. Topology optimization for thermo-mechanical compliant actuators using mesh-free methods. *Eng. Optim.* **2009**, *41*, 753–772. [[CrossRef](#)]
4. Li, Q.; Steven, G.P.; Xie, Y.M. Thermo-elastic topology optimization for problems with varying temperature fields. *J. Therm. Stress.* **2001**, *24*, 347–366. [[CrossRef](#)]
5. Deng, J.D.; Yan, J.; Cheng, G.D. Multi-objective concurrent topology optimization of thermo-elastic structures composed of homogeneous porous material. *Struct. Multidiscip. Optim.* **2013**, *47*, 583–597. [[CrossRef](#)]
6. Deaton, J.D.; Grandhi, R.V. Stiffening of restrained thermal structures via topology optimization. *Struct. Multidiscip. Optim.* **2013**, *48*, 731–745. [[CrossRef](#)]
7. Haney, M.A.; Grandhi, R.V. Consequences of material addition for a beam strip in a thermal environment. *AIAA J.* **2009**, *47*, 1026–1034. [[CrossRef](#)]
8. Le, C.; Norato, J.; Bruns, T.; Ha, C.; Tortorelli, D. Stress-based topology optimization for continua. *Struct. Multidiscip. Optim.* **2010**, *41*, 605–620. [[CrossRef](#)]
9. Cheng, G.D.; Guo, X. ϵ -relaxed approach in structural topology optimization. *Struct. Optim.* **1997**, *13*, 258–266. [[CrossRef](#)]
10. Wang, X.; Wang, J.; Wang, X.; Yu, C.J. A pseudo-spectral fourier collocation method for inhomogeneous elliptical inclusions with partial differential equations. *Mathematics* **2022**, *10*, 296. [[CrossRef](#)]
11. Bruggi, M.; Venini, P. A mixed FEM approach to stress-constrained topology optimization. *Int. J. Numer. Methods Eng.* **2008**, *73*, 1693–1714. [[CrossRef](#)]
12. Gao, J.; Xue, H.; Gao, L.; Luo, Z. Topology optimization for auxetic metamaterials based on isogeometric analysis. *Comput. Meth. Appl. Mech. Eng.* **2019**, *352*, 211–236. [[CrossRef](#)]
13. Chen, Z.; Long, K.; Wen, P.; Nouman, S. Fatigue-resistance topology optimization of continuum structure by penalizing the cumulative fatigue damage. *Adv. Eng. Softw.* **2020**, *150*, 102924. [[CrossRef](#)]
14. Yue, X.X.; Wang, F.J.; Hua, Q.S.; Qiu, X.Y. A novel space–time meshless method for nonhomogeneous convection–diffusion equations with variable coefficients. *Appl. Math. Lett.* **2019**, *92*, 144–150. [[CrossRef](#)]
15. Yang, R.J.; Chen, C.J. Stress-based topology optimization. *Struct. Multidiscip. Optim.* **1996**, *12*, 98–105. [[CrossRef](#)]
16. Guo, X.; Zhang, S.W.; Wang, M.Y.; Wei, P. Stress-related topology optimization via level set approach. *Comput. Meth. Appl. Mech. Eng.* **2011**, *200*, 3439–3452. [[CrossRef](#)]
17. Zhang, W.S.; Guo, X.; Wang, M.Y.; Wei, P. Optimal topology design of continuum structures with stress concentration alleviation via level set method. *Int. J. Numer. Methods Eng.* **2013**, *93*, 942–959. [[CrossRef](#)]
18. Deaton, J.D.; Grandhi, R.V. Stress-based design of thermal structures via topology optimization. *Struct. Multidiscip. Optim.* **2016**, *53*, 253–270. [[CrossRef](#)]
19. Liu, J.; Qing, Q.; Deng, Y.; Wen, G.; Yin, H. Fatigue reliability study on T-welded component considering load shedding. *Fatigue Fract. Eng. Mater. Struct.* **2015**, *38*, 780–788. [[CrossRef](#)]
20. Li, X.Q.; Zhao, Q.H.; Zhang, H.X.; Zhang, T.Z.; Chen, J.L. Robust topology optimization of periodic multi-Material functionally graded structures under loading uncertainties. *CME5-Comput. Model. Eng. Sci.* **2021**, *127*, 683–704. [[CrossRef](#)]
21. Glowacz, A. Fault diagnosis of electric impact drills using thermal imaging. *Measurement* **2021**, *171*, 108815. [[CrossRef](#)]
22. Rabcan, J.; Levashenko, V.; Zaitseva, E.; Kvassay, M.; Subbotin, S. Non-destructive diagnostic of aircraft engine blades by fuzzy decision tree. *Eng. Struct.* **2019**, *197*, 109396. [[CrossRef](#)]
23. Kharbanda, G.; Olhoff, N.; Mohamed, A.; Lemaire, M. Reliability-based topology optimization. *Struct. Multidiscip. Optim.* **2004**, *26*, 295–307. [[CrossRef](#)]
24. Jung, H.S.; Cho, S. Reliability-based topology optimization of geometrically nonlinear structures with loading and material uncertainties. *Finite Elem. Anal. Des.* **2004**, *41*, 311–331. [[CrossRef](#)]
25. Zhao, Q.H.; Zhang, H.X.; Zhang, T.Z.; Hua, Q.S.; Yuan, L.; Wang, W.Y. An efficient strategy for non-probabilistic reliability-based multi-material topology optimization with evidence theory. *Acta Mech. Solida Sin.* **2019**, *32*, 803–821. [[CrossRef](#)]
26. Silva, M.; Tortorelli, D.A.; Norato, J.A.; Ha, C.; Bae, H.-R. Component and system reliability-based topology optimization using a single-loop method. *Struct. Multidiscip. Optim.* **2010**, *41*, 87–106. [[CrossRef](#)]
27. Zhao, Q.H.; Chen, X.K.; Ma, Z.D.; Lin, Y. A Comparison of deterministic, reliability-based topology optimization under uncertainties. *Acta Mech. Solida Sin.* **2016**, *29*, 31–45. [[CrossRef](#)]
28. Wang, C.; Wang, F.J.; Gong, Y. Analysis of 2D heat conduction in nonlinear functionally graded materials using a local semi-analytical meshless method. *AIMS Math.* **2021**, *6*, 12599–12618. [[CrossRef](#)]

29. Gao, T.; Zhang, W.H. Topology optimization involving thermo-elastic stress loads. *Struct. Multidiscip. Optim.* **2010**, *42*, 725–738. [[CrossRef](#)]
30. Aoues, Y.; Chateaneuf, A. Benchmark study of numerical methods for reliability-based design optimization. *Struct. Multidiscip. Optim.* **2010**, *41*, 277–294. [[CrossRef](#)]
31. Niccolai, A.; Caputo, D.; Chieco, L.; Grimaccia, F.; Mussetta, M. Machine learning-based detection technique for NDT in industrial manufacturing. *Mathematics* **2021**, *9*, 1251. [[CrossRef](#)]
32. Wang, F.J.; Zhao, Q.H.; Chen, Z.T.; Fan, C.M. Localized Chebyshev collocation method for solving elliptic partial differential equations in arbitrary 2D domains. *Appl. Math. Comput.* **2021**, *397*, 125903. [[CrossRef](#)]
33. Lee, S.H.; Chen, W. A comparative study of uncertainty propagation methods for black-box-type problems. *Struct. Multidiscip. Optim.* **2009**, *37*, 239–253. [[CrossRef](#)]
34. Hasofer, A.M.; Lind, N.C. Exact and invariant second moment code format. *J. Eng. Mech.* **1974**, *100*, 111–121. [[CrossRef](#)]
35. Maute, K.; Frangopol, D.M. Reliability-based design of MEMS mechanisms by topology optimization. *Comput. Struct.* **2003**, *81*, 813–824. [[CrossRef](#)]
36. Wang, L.; Xia, H.J.; Zhang, X.Y.; Lv, Z. Non-probabilistic reliability-based topology optimization of continuum structures considering local stiffness and strength failure. *Comput. Meth. Appl. Mech. Eng.* **2019**, *346*, 788–809. [[CrossRef](#)]
37. Xiao, M.; Zhang, J.H.; Gao, L. A system active learning Kriging method for system reliability-based design optimization with a multiple response model. *Reliab. Eng. Syst. Saf.* **2020**, *19*, 106935. [[CrossRef](#)]
38. Bruns, T.E.; Tortorelli, D.A. Topology optimization of non-linear structures and compliant mechanisms. *Comput. Meth. Appl. Mech. Eng.* **2001**, *190*, 3443–3459. [[CrossRef](#)]
39. Svanberg, K. The method of moving asymptotes—a new method for structural optimization. *Int. J. Numer. Methods Eng.* **1987**, *24*, 359–373. [[CrossRef](#)]